Journal of Aircraft
Vol. 44, No. 2, March–April 2007

Effect of Swirl Flows in Aeronautical Mix Manifolds

R. Bourlart*
Daher Group, 41400 Saint Julien de Chédon, France
R. Weber† and J. Hureau‡
Laboratoire de Mécanique et d'Energétique, 45072 Orléans Cedex 02, France
and
F. Landais§
Daher Group, 41400 Saint Julien de Chédon, France

DOI: 10.2514/1.23916

This paper studies the mixing manifold, a specific component of aeronautical low-pressure air conditioning systems, in an effort to optimize cabin thermal regulation. This component homogenizes hot and cold air fluxes using turbulent, incompressible swirl flows. We identify several flow regimes in the manifold, depending on boundary conditions and the absence or presence of flow control devices in the manifold. A scaled-down model (0.445) is first validated in terms of kinetic and thermal similarity, and is then used for the experimental part of the study. We then identify physical phenomena by acoustic analyses and numerical computational fluid dynamics simulations. We found a precessing vortex breakdown to be present in several of the configurations studied, creating high acoustic noise and vibratory fatigue problems. Solutions are then proposed to avoid these sources of passenger discomfort. The mixing manifold spatial dimensions are also reduced, striking a good compromise between flow-mixing quality, pressure loss, and acoustic noise, to meet aeronautical weight reduction specifications for composite structures.

Nomenclature

A_1, A_2	=	singularity inlet and outlet sections
Cp	=	heat capacity
D	=	diameter (mixing manifold or linear duct)
d	=	distance between two opposing inlet axes when mixing manifold inlets are parallel
Ec	=	Eckert number
e	=	total energy
f	=	frequency
K	=	dimensionless factor
L	=	linear duct length
n	=	number of inlets
P	=	mean static pressure
Pr	=	Prandtl number
p	=	local static pressure
Re	=	Reynolds number
r	=	local radial coordinate
S	=	swirl number
T	=	temperature
T_a	=	averaged temperature
T_{pack}	=	pack inlet temperature
$T_{\text{recirculation}}$	=	recirculation inlet temperature
t	=	time
u	=	local velocity
V, V'	=	mean velocity
w_φ	=	tangential velocity
w_x	=	axial velocity
x	=	local space coordinate
γ	=	ratio of heat capacities
ΔP	=	total pressure loss
δ_{ij}	=	Krönecker delta symbol
ε	=	linear duct roughness
Θ	=	dimensionless temperature
θ	=	dimensionless temperature (similarity rules)
λ	=	heat conductivity
μ	=	dynamic viscosity
ρ, ρ'	=	density
Σ	=	section
σ_{ij}	=	shear stress tensor component
φ, φ'	=	functions defining, respectively, the linear and singular pressure loss coefficient

Subscripts

i, j	=	spatial coordinates
k	=	inlet or outlet number
M	=	scaled-down model
R	=	full-scale model

I. Introduction

AIRCRAFT manufacturers have been researching aircraft cabin ventilation for many years to improve passenger comfort. Their primary goal is to achieve a good distribution of air flow at the right temperature in the cabin. Moreover, considering the progress that has been made on the main noise sources (i.e., from the engines and noises of aerodynamic origin), secondary noise generators are becoming relatively more audible, and this is especially true for the low-pressure air conditioning system (aircraft ventilation, pressurization, and avionics cooling).

The present study deals with low-pressure air distribution systems in terms of fluid mechanics and aeroacoustics. When hot and cold turbulent, incompressible swirl flows are mixed, they can create precessing vortex breakdowns that generate harmful acoustic emissions. The aim here is to analyze a common thermal regulation

Received 15 March 2006; revision received 7 September 2006; accepted for publication 25 September 2006.

*Research Engineer, Daher, New and Sustainable Activities Department, 23 Route de Tours, 41400 Saint Julien de Chédon, France; r.bourlart@daher.com.

†Doctor, Laboratoire de Mécanique et d'Energétique, Département Mécanique des Fluides, 8 rue Léonard de Vinci, 45072 Orléans Cedex 02, France; regine.weber@univ-orleans.fr.

‡Professor, Laboratoire de Mécanique et d'Energétique, Département Mécanique des Fluides, 8 rue Léonard de Vinci, 45072 Orléans Cedex 02, France; jacques.hureau@univ-orleans.fr.

§Research Engineer, New and Sustainable Activities Department, 23 Route de Tours, 41400 Saint Julien de Chédon, France; f.landais@daher.com.

component called the mixing manifold, and then to optimize it from the space allocation viewpoint and decrease its noise pollution.

In addition to fan vibrations, the linear pneumatic ducts and singularities generate and propagate pressure fluctuations with harmful effects in terms of acoustic comfort, noise standards, and vibratory fatigue risks. Fluid-structure couplings can also deteriorate ducts and other specific components, even when they are at a great distance from the excitation source, because of the acoustic waves propagation. Consequently, aeroacoustic aspects have to be considered if we want to achieve performance levels in accordance with aeronautical specifications. Moreover, it seems preferable that these problems be solved at their source, rather than using expensive acoustic mufflers with their associated weight penalties.

Aircraft thermal regulation is partially ensured by the mixing manifold. Its function is to mix “recirculating” hot air flows from the cabin and cockpit (and consequently recycled) with cold air flows (new air from outside the plane, picked off the engines, and conditioned by packs). The resulting mixed air is then distributed to the various air distribution circuits. The pack inlets ensure sufficient oxygen renewal, but also the global aircraft cooling. Thermal homogeneity is achieved at the manifold outlets at the expense of mass and space allocation. Moreover, a temperature adjustment may be made among outlets using hot air injectors to compensate for thermal fluctuations and various thermal losses of the circuits. These components should be avoided because of their harmful aeroacoustic effects.

A secondary function of the mixing manifold is to prevent fog from arising in the cabin as the very humid recycled hot air mixes with the cold air. This it does by accelerating water condensation during the mixing process.

Many papers have been written on the mixing manifold. In 1985, Eggebrecht et al. [1] described this complex component such as it can be seen nowadays on Airbus and Boeing aircraft. The cylindrical section of the mixing manifold and the different inlets are designed in such a way that the flows are subjected to a sudden expansion, which is the first stage of flow homogenization.

The inlets, which are tangential to the main cylinder, create a swirl flow that accelerates the mixing but also extracts the water by centrifugal forces. Small deflectors fixed inside the manifold trap water droplets and guide them to a drain at the bottom. Honeycomb structures on the top optimize the mixing. Today’s mixing manifolds are somewhat different because of the presence of other turbulence generators such as combs and diaphragms. These additional components are limited, however, because of weight and manufacturing problems.

Swirl flows and associated mechanisms [breakdown and precessing vortex breakdown (PVB)] are used to mix hot and cold air flows quickly in a mixing manifold. The swirl flows result from an azimuthal velocity component, which is imposed on the flow by various swirl generators: axial or radial guide vanes, helical inserts, or rotating tubes, for example. Axial vanes are set on a central hub, at a certain angle to the axial direction of the duct [2,3]. Radial vanes are generally mounted between two disks, and generate more intense swirls [4].

These different swirlers, involving variable heat and mass transfers, are usually penalizing in terms of pressure loss. Powerful fans are thus needed [4]. In aeronautical mixing manifolds, manufacturers tend to prefer tangential inlets, which are more advantageous from this point of view. A use of the swirl flow is to increase fluid-to-solid heat transfer, which it does by increasing axial velocity and decreasing boundary layer thickness, while raising turbulence levels at the same time [5]. The averaged kinetic energy and turbulence levels are then large.

It should be noted that most papers do not deal with the mixing between hot and cold air fluxes, but rather with combustion optimization [6]. In 1976, Razgaitis and Holman [7] proposed various ways of understanding heat transfer in heat exchangers. More recently, Martemianov and Okulov [8] showed that several flow states exist in the presence of swirl. They emphasize the fact that the traditional empirical models are generally unsatisfactory because the swirl characteristics (which are continuous if the flow properties are maintained throughout the entire section test, and otherwise decaying) and swirl intensity do not fully explain the heat and mass transfers. In fact, it is essential to know whether the vortex has left- or right-handed symmetry, which correspond to a given axial velocity profile state (jet or wakelike). The two symmetries may even exist with the same integral flow parameters (flow rate, flow circulation, angular momentum, and energy). Lucca-Negro and O’Doherty [9] explain that during vortex breakdown, the transition between these two states can occur even if the Reynolds and swirl numbers are constant.

Vortex breakdown corresponds to the stagnation of the vortex core, followed by an expanding structure (of the bubble or spiral type). The various swirl number definitions usually consider axial and tangential velocities but neglect any turbulence fluctuations (pressures and velocities are time-averaged), whereas some of these definitions consider only the swirl generator’s geometric parameters. Alekseenko et al. [10] describe the main helical structures theoretically and experimentally. With the same swirl and Reynolds numbers, and specific boundary conditions, they observe a PVB with an unsteady helical vortex core. Other conditions lead to a steady rectilinear vortex core. As integral parameters are insufficient for determining the flow regime, our study requires particle image velocimetry (PIV) visualizations, CFD simulations, and acoustic measurements to identify the type of symmetry and the flow characteristics in the mixing manifold.

An experimental test campaign was first conducted to analyze the model mixing manifold characteristics in the absence of internal devices. In fact, the geometries used on today’s aircraft have been designed empirically. Our prototype geometry is based on the Airbus A340-600 design, which is representative of the latest mixing and space allocation improvements.

We chose to work on scaled-down models ($L_M/L_R = D_M/D_R = 0.445$) so that we could use less powerful fans. However, when using a reduced model, the thermal and kinetic similarity rules first have to be validated. Then, after a preliminary study using PIV visualizations, frequency analyses, and CFD numerical simulations, we were able to validate the experimental measurements (thermal and pressure loss) and identify the flow regime.

The last stage of the study consisted of optimizing the mixing manifold from the weight and space allocation viewpoints. Industrial constraints are imposed when doing this. The mixing manifold cannot contain baffles, and there must be no greater pressure losses than in previous designs. The main optimization parameters are the inlet orientations, the swirl degree, the manifold height, the outlet boundary conditions (presence of diaphragms), and the presence of internal devices.

II. Investigation Possibilities

A. Experimental Setup

Two prototypes were tested during the mixing manifold qualification and similarity rule validation stages: one full-scale and one 0.445-scale prototype (Fig. 1). The orientation of the two packs (Ps1 and Ps2) and the two recirculation inlets (R1 and R2) are in accordance with the geometry of the A340-600 mixing manifold. Only the outlets are modified. Their omnidirectional positions avoid any specific flow orientation at the top of the mixing manifold. The pack inlets are supplied with fresh air (about 20°C) by centrifugal fans (Fig. 2), and recirculation ones with hot air (60°C) by axial fans coupled to thermal resistors. Velocities and pressures are measured with a pitot tube (3 mm diam) connected to a velocimeter (TSI Velocicalc plus). The average velocity in a section (and also the flow rate) is calculated according to the ISO 3966 standard (NFX 10-112) [11]. A Tchebysheff log method is applied at least 10 diameters after the components for the measurements. Linear ducts are then used upstream of the pitot locations. The temperature is recorded with J-type thermocouples (error of 0.1°C for the study range). The average temperature over a section is found using four equidistant thermocouples (0.7 mm diam) mounted on an aerodynamically profiled rod. The system blockage is estimated at 5% of the total section. The maximum pack temperature variation, which is linked

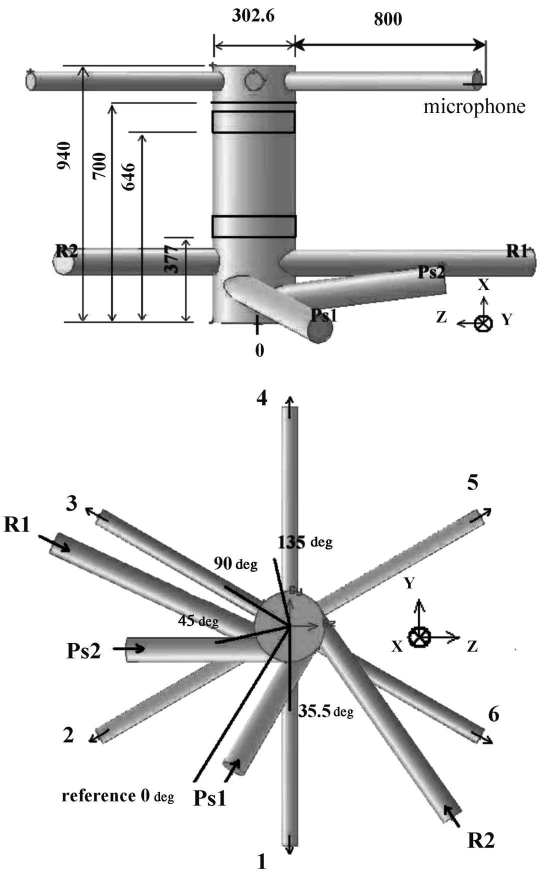

Fig. 1 Mixing manifold prototype (scale 0.445, size in mm), front and bottom views.

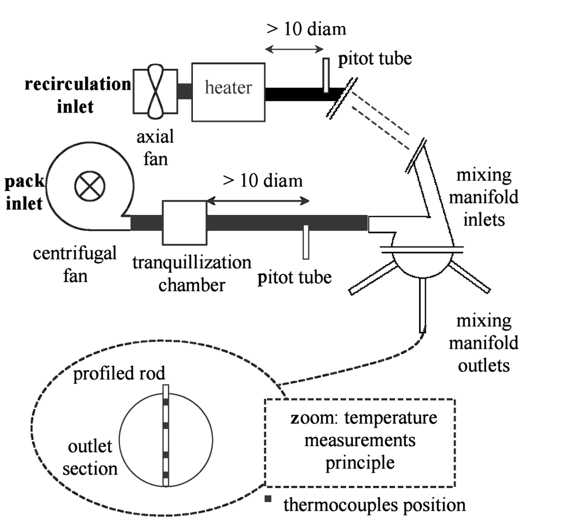

Fig. 2 Principles of the experimental test bench (pack, recirculation inlets, and outlets).

directly to that of the ambient temperature, is 0.3°C. All these precautions enabled us to achieve a maximum outlet temperature fluctuation of 0.3°C. Figure 3 gives a definition of the geometry and locations of the internal devices.

Acoustic tests were carried out with a microphone (1/2 in. diam) protruding into the flow at one of the mixing manifold outlets, 800 mm downstream from the tank of the mixing manifold (Fig. 1). A microphone nose cone (G.R.A.S. Sound & Vibration type RA0020, Fig. 4) improves the measurements (by suppressing the aeroacoustic noise due to the protective screen) and decreases the production of turbulence. It is connected to an amplifier with a high pass filter of 0.3 Hz and a gain of 0 dB (linear weighting). The amplifier is

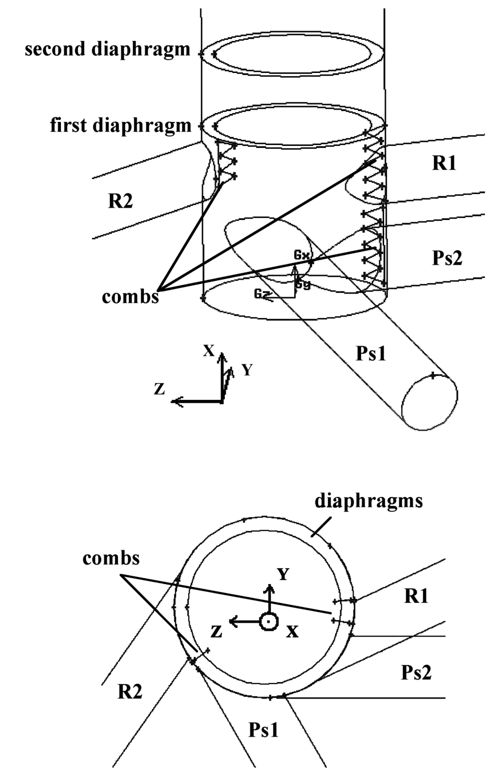

Fig. 3 Internal devices at bottom of mixing manifold, front and top views.

Fig. 4 Microphone nose cone.

connected to an acquisition computer that analyzes the power spectrum density (PSD) with a sensitivity setting of 10 mV/Pa, 100 Hz bandwidth, oversampling of 10, and a rectangular window for the PSD calculation. The maximum sensitivity of 1000 mV/Pa and the bandwidth of 10 Hz were used only for tests on the full-scale model. This was because the frequencies in this case are very low (below 20 Hz), which requires special settings to pick up the phenomena.

The optimization stage required new prototype designs. Contrary to the A340-600 mixing manifold, all the inlets were placed in the same plane, and the injection angle was varied between 0 and 90 deg in steps of 22.5 deg (tangential inlets correspond to an injection angle of 0 deg, Fig. 5). The effect of the swirl number on the mixing phenomena was then studied with the five prototypes. Because the mixing manifold height was another variable parameter, the model was built in different parts.

All measurements were carried out under the same volumetric flow rate conditions. The pack inlet flow rate was 210 l/s, whereas the recirculation rate was 150 l/s. The ratio Ps1/R1 is set as a passenger comfort criterion. The aeronautical specifications, however, were not met because our fans did not have enough power to reach the nominal conditions.

The mixing manifold qualification and optimization stages involved studying the effects with and without combs and diaphragms inside the manifold (Fig. 3), and by varying the manifold height and the flow injection angles. The inlet and outlet diameters were left fixed, as were the ambient pressure and temperature conditions.

B. Numerical Simulations

The numerical simulations, carried out with the Fluent software, improved our understanding of the swirl flow regimes in the mixing manifold. A parametric analysis of the code is needed to achieve the best prediction. The two classical two-equation models (k–ε and k–ω), though economical in terms of computation time, are nonetheless ill-suited to simulations of PVB phenomena. And so, we chose the unsteady Reynolds-averaged Navier–Stokes (U-RANS) formulation with a Reynolds stress model (RSM) with seven equations, using the default parameters, which was developed to improve formulations using the Newton viscosity hypothesis, and to find a quasi-universal closed model for the Reynolds tensor [12].

Unfortunately, the RSM causes numerical divergences and consumes prohibitive computation time. Concerning the pressure-velocity coupling, a simple pressure correction method was used, and a second-order upwind scheme was imposed for the momentum, energy, turbulence kinetic energy, turbulence dissipation rate, and Reynolds stresses discretizations.

To capture a periodic phenomenon in the mean flow using U-RANS, the averaging computation period has to be much smaller than the time scale of the unsteady mean motion. And so, a steady-state calculation with a standard k–ε model was first carried out to obtain the initial conditions for the unsteady RSM, to ensure convergence. After a few iterations, corresponding to a few periods of the phenomenon being studied, a periodic solution appeared. The frequency of a PVB, if one existed, was then found by monitoring the velocity at several points inside the mixing manifold, the mean temperature at outlet sections, and the mean static pressure at the inlet sections.

III. Similarity Rules

A. Theoretical Analysis

To limit the scale effects (that is, the physical phenomena present on the scaled-down model but absent on the full-scale), the scale factor is limited to 0.445. The fluid is then incompressible for both scales. The swirl chamber exhibits several flow regimes. These regimes are mainly dependent on the Reynolds numbers, swirl numbers, and the swirl generator used (guide vanes or tangential inlets). In a first approximation, we assume that the flow regime is the same at both scales if the similarity rules comply.

In the fluid mechanics analysis, the Navier–Stokes momentum equation is used. The dimensionless analysis (the general compressible case) leads to Reynolds similarity, with the Einstein notation

$$\frac{\partial \rho u_i}{\partial t} + \frac{\partial}{\partial x_j}\left(\rho u_i u_j + P\delta_{ij} - \frac{1}{Re}\mu\sigma_{ij}\right) = 0 \qquad (1)$$

The Reynolds number is referenced to the hydraulic diameter.

The flow phenomena encountered in our study have to be taken into account in the similarity rules. These can be represented partially by the swirl number. Many authors, such as Alekseenko et al. [10], define the swirl number as follows (using our notation):

$$S = \frac{2\int_\Sigma \rho w_\varphi w_x r \,\mathrm{d}\Sigma}{D\int_\Sigma (p + \rho w_x^2)\,\mathrm{d}\Sigma} \qquad (2)$$

Equating this swirl number for the two scale models leads to an incoherence, so kinetic similarity could be not validated. Yilmaz et al. [4] thus gave a definition of the convection coefficient (referenced to the Nusselt number) between a swirl flow and a solid boundary, using the Reynolds, Prandtl, and swirl numbers. In Yilmaz's study, the swirl number is dependent only on the orientation of the generators (geometric definition). Correlations between experimental tests and analytical formulations of convective phenomena then yield good results.

We decided to apply this definition in our own study. However, the geometric swirl number is difficult to characterize in the case of tangential manifold inlets. The definition proposed by Alekseenko et al. [10] for a square-section swirl chamber is thus generalized for our geometries. If we assume that all inlets have the same diameter and flow rate, we get

$$S = \frac{Dd}{\sum_k D_k^2} \qquad (3)$$

in which d is defined in Fig. 5, and D_k is the diameter of the kth inlet duct ($k \in [1, n]$). As the geometric similarity is upheld between the two scales, the geometric swirl numbers are equal.

For variable inlet flow rates and diameters, we got a different swirl number definition and again verify that the swirl numbers were equal. We concluded that the previous uncertainties concerning the kinetic similarity validity can be qualified.

Other definitions exist for the swirl number. For example, the relation including integral quantities [Eq. (2)] is often replaced with the ratio of the maximum azimuthal velocity to the maximum axial velocity [13,14]. The Reynolds similarity then entails the equal swirl numbers at the two scales.

By kinetic similarity, the pressure loss with the full-scale model is deduced from that of the scaled-down model. Let us consider, for example, that the manifold pressure loss can be divided into linear and singular pressure losses. Dimensional analysis then gives us

$$\frac{\Delta P_R}{\Delta P_M} = \frac{(L_R/D_R)\varphi_R(Re_R, \varepsilon_R/D_R)\rho_R V_R^2 + \varphi'_R(A_{1R}, A_{2R})\rho'_R V_R'^2}{(L_M/D_M)\varphi_M(Re_M, \varepsilon_M/D_M)\rho_M V_M^2 + \varphi'_M(A_{1M}, A_{2M})\rho'_M V_M'^2} \qquad (4)$$

If the geometric and kinetic similarities are verified, and if the ratio of scaled-down/full-scale model roughness is 0.445, then the φ_M and φ_R functions are equal. We formulate the same conclusion for the φ' function. The swirl flow involves an additional pressure loss in the ducts. For this, we deduce Eq. (5) according to the Rayleigh method (all the inlets are assumed to be of the same diameter, D_k):

$$\frac{\Delta P_R}{\Delta P_M} = \frac{(L_R/D_R)\varphi_R(Re_R, \varepsilon_R/D_R, d_R/D_R, nD_{kR}/D_R)\rho_R V_R^2 + \varphi'_R(A_{1R}, A_{2R})\rho'_R V_R'^2}{(L_M/D_M)\varphi_M(Re_M, \varepsilon_M/D_M, d_M/D_M, nD_{kM}/D_M)\rho_M V_M^2 + \varphi'_M(A_{1M}, A_{2M})\rho'_M V_M'^2} \qquad (5)$$

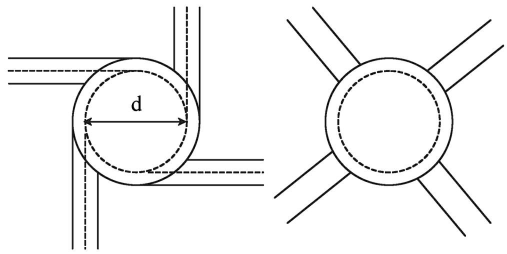

Fig. 5 Definition of the injection angle.

As concerns thermal similarity, the corresponding formula is the energy equation. Dimensionless analysis for incompressible flows yields

$$\frac{\partial \rho e}{\partial t}+\frac{\partial}{\partial x_j}\left[(\rho e+P)u_j-\frac{1}{Re}\mu\sigma_{ij}u_i-\frac{1}{\gamma-1}\frac{\mu}{Pr\,Re}\frac{\partial T}{\partial x_j}\right]=0 \tag{6}$$

The similarity can then be validated if equalities are respected between the Reynolds and the Prandtl numbers ($Pr=\mu Cp/\lambda$). Experiments have been performed with identical inlet temperatures for the two scales. The Prandtl numbers are then identical and, according to the correspondence of the Reynolds numbers, the thermal similarity is respected. Because the flow regime is turbulent, the molecular transport (characterized by the Prandtl number) is negligible compared with the turbulent mixing. Consequently, we do not need equal Prandtl numbers at the two scales to validate thermal similarity.

We may note that the dimensionless energy equation, using enthalpy, can be expressed as

$$\rho Cp\left(\frac{\partial T}{\partial t}+T_{,j}u_j\right)=Ec\left(\frac{\partial p}{\partial t}+p_{,j}u_j\right)+\frac{Ec}{Re}u_{i,j}\sigma_{ij}+\frac{1}{Re\,Pr}(\lambda T_{,j})_{,j} \tag{7}$$

in which $Ec=V^2/Cp\theta$ is the Eckert number. Thus, similarity is not upheld for the Eckert number. However, the compressibility and shearing heat transfer phenomena, which are represented by the Eckert number, can nonetheless be neglected here because of the low Mach numbers. The experimental setup assumes that the mixing manifold walls are adiabatic, so that the radiation and heat conduction phenomena are neglected. Moreover, free convection does not appear, so that the Grashoff number has no effect on the mixing. Indeed, the ratio between the Grashoff number and the Reynolds number calculated for example at the bottom of the mixing manifold, at the level of a recirculation inlet, is sufficiently low (2.4×10^{-4}).

In the introduction, we noted that aeroacoustic phenomena might exist in a mixing manifold. A similarity rule must then be established for the time scale. This can be done using the standard relation between velocity, length, and time:

$$V_M=\frac{L_M}{t_M}\quad\text{and}\quad V_R=\frac{L_R}{t_R} \tag{8}$$

in which $L_M=0.455L_R$. Applying the Reynolds similarity, the velocity in the scaled-down model can be deduced from the properties of the full-scale flow:

$$V_M=\frac{\rho_R}{0.445\rho_M}\frac{\mu_M}{\mu_R}V_R \tag{9}$$

The frequency f_M of the PVB in the scaled-down model can be then defined as

$$f_M=\frac{(\mu_M/\mu_R)(\rho_R/\rho_M)f_R}{0.445^2} \tag{10}$$

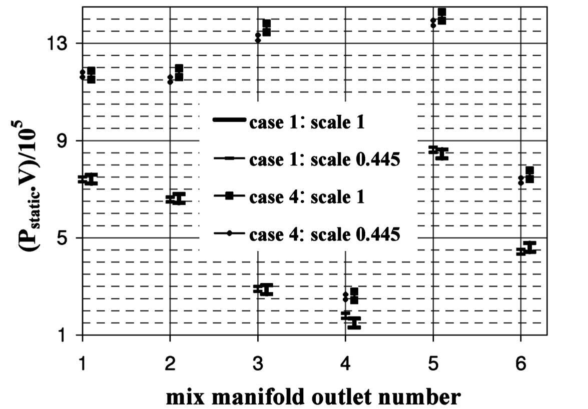

Fig. 6 Similarity rule validation considering velocity measurement uncertainties.

Lastly, the use of tranquilization boxes downstream of the fans (suppressing, for example, the swirl flow of axial fans) and honeycomb structures (leading to a quasi-homogeneous and isotropic turbulence rate) allow us to use the same inlet flow conditions for the scaled-down and full-scale models.

B. Experimental Validation

The velocity measurements are validated by verifying the flow rate balance between the manifold inlets and outlets. The difference in the flow rates is less than 1% for the scaled-down model and 2% for the full-scale.

Reynolds similarity is imposed on the real case and model inlets: the product of the static pressure and the velocity for a given temperature is fixed at each inlet. Reynolds similarity is then verified at the outlets: the full-scale static pressure-velocity products are compared with the 0.445-scale measurements, using similarity rules, in Fig. 6 and Table 1, showing the uncertainties due to the apparatus and testing techniques.

For the velocity measurements, by velocimeter gauging, the maximum error is ±0.4 m/s for the range [2–30] m/s (this spans the study range), and the resolution is 0.1 m/s. Moreover, the Tchebysheff log method includes an absolute error on the averaged velocity in a section from -0.4 to $+3.6\%$.

All these reasons explain differences that appear in the flow rate balance and the range of uncertainties in Fig. 6 and Table 1. The atmospheric pressures and temperatures were recorded for each test. There are also no additional errors caused by the atmospheric pressure and the ambient temperature variations. Many cases were studied to test the effects of the diameters of outlet diaphragms and the number of inlets supplied (Fig. 6 does not show all of the results).

For all the configurations studied, considering the uncertainties, the pressure-velocity products at the outlets are in good agreement between the two scales. The kinetic similarity thus appears to be valid.

We can deduce the full-scale model pressure loss from the scaled-down model data. In the reasoning given earlier, we considered the scaled-down model data to be broken down into linear and singular parts [Eq. (5)]. In a first approximation, the φ and φ' functions are inseparable between the two scales (the scaled-down model roughness is less than that of the full-scale model, but the 0.445 scale

Table 1 Cases tested for similarity rule validation

Case	Exit diaphragm diameter, mm, scale 1						Inlet used	
	1	2	3	4	5	6	Ps1	Ps2
1	——	——	100	70	——	120	——	x
2	——	——	——	70	——	120	——	x
3	——	——	——	——	——	——	——	x
4	——	——	——	70	——	120	x	x
5	——	——	100	70	——	120	x	x

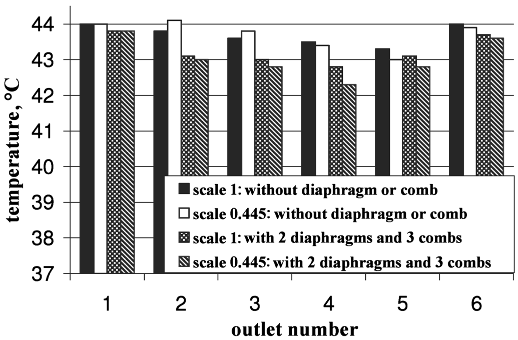

Fig. 7 Mixing manifold outlet temperatures: four inlets.

factor is not followed, which introduces an error). The main problem consists in determining the product ρV^2 for homologous points between the two scales (K is a factor independent of pressure and velocity), as

$$\rho_M V_M^2 = K \rho_R V_R^2 \tag{11}$$

to obtain an analytical formula relating ΔP_M to ΔP_R. The equal Reynolds numbers do not allow us to deduce the formula of Eq. (11). And so, we simplify the problem by neglecting the thermal and pressure differences between the two scales for homologous points, and thereby obtain

$$\rho_M V_M^2 = \frac{1}{0.445^2} \rho_R V_R^2 \tag{12}$$

We then deduce, from Eq. (5), the final relation:

$$\Delta P_M = \frac{\Delta P_R}{0.445^2} \tag{13}$$

The full-scale model pressure loss is deduced from that of the scaled-down model with a maximum error of 5% for all tests. This confirms the validity of kinetic similarity and the associated assumptions (pressure and temperature effects, geometric swirl number, and linear/singular pressure loss breakdown). We reach the same conclusions if the pack and recirculation flow rates are decreased at the same Ps1/R1 ratio (148 1/s for pack and 150 1/s for recirculation).

Thermal similarity is automatically validated because the same fluids, at the same temperatures, are used with the scaled-down and full-scale models. Verifications were carried out on the temperature profiles at the outlets (considering the uncertainties) and good agreement was found between the two scales (Fig. 7).

To test the validity of the aeroacoustic similarity (Table 2), tests were carried out on a mixing manifold supplied by four inlets, with and without internal devices, and with standard outlets (a PVB then exists). For example, measurements on the scaled-down model show the presence of a PVB at a root frequency of 39.7 Hz (the first harmonic is at 78.7 Hz) for a mixing manifold with no internal devices. Equation (10) then predicted a PVB frequency of 8.3 Hz (16.3 Hz for the first harmonic) for the full-scale model. Measurements on the full-scale model yielded 7.9 and 16 Hz, respectively. Because the error was no more than 5 % (Table 2), we concluded that the aeroacoustic similarity was valid. We should point out that the highest error for a manifold with three combs is due to the fact that the Reynolds numbers do not comply (according to the Reynolds similarity) for two inlets. An error of 15% was estimated on it.

Table 2 Comparison between theoretical and measured PVB frequencies for several mixing manifold configurations

	Theoretical frequency scale 1, Hz	Measured frequency scale 1, Hz	Error, %
Mix manifold without internal devices	8.3	7.9	4.8
Mix manifold with 3 combs	5.8	5.1	12.1
Mix manifold with 3 combs and a diaphragm	5	4.9	2
Mix manifold with 3 combs and two diaphragms	5.1	5.3	3.8

From the preceding results, we deduced that the aeroacoustic, kinetic, and thermal similarities were valid. The orientation and the number of supplied inlets, the outlet diaphragms, and the internal devices do not affect the similarity rules. Moreover, no scale, compressible, or shearing heat effects exist, and the only necessity is that the geometric swirl numbers comply. Molecular transport is less than the turbulent mixing. The flow regimes are the same at the two scales.

On the other hand, the invalid acoustic similarity constitutes a limitation on the use of a scaled-down model. That is, let us assume that the full-scale manifold exhibits Helmholtz resonance. Then, in the scaled-down model, the resonance frequency is twice that of the full-scale (2.247, precisely). However, kinetic similarity requires that an aeroacoustic frequency on the scaled-down model (such as a PVB phenomenon) be four times higher than on the full-scale. Consequently, full-scale resonance (the PVB frequency is equal to the Helmholtz frequency) is not present on the model. There can, however, be resonance harmonics.

IV. Quantification of Mixing Manifold Pneumatic Performances

Because the similarity rules applied, experimental tests were carried out only on the scaled-down model. The aim of the following sections is to quantify the mixing manifold by studying the mixing quality, the function of the internal devices (diaphragms and combs positioned in the main cylinder, Fig. 3) of the outlet diaphragms and of the mixing manifold height. The reference case is a nonreduced A340-600 mixing manifold without internal device, outlet diaphragm, and top outlet. The reference pressure loss is 1820 Pa. Let us consider that the mixing manifold exhibits good thermal mixing if the maximum thermal fluctuation at the outlets does not exceed 1.5°C.

A. Effects of Combs and Diaphragms

Figure 8 and Table 3 show the temperature distributions at the outlets of the mixing manifold. The averaged temperature but also the nondimensional temperature $[\Theta = (T_a - T_{\text{pack}})/(T_{\text{recirculation}} - T_{\text{pack}})]$ are given for each outlet section. Cases 1–4 show that asymmetrical outlets have no effect on the mixing quality. Consequently, the pressure losses in the pneumatic circuits connected to the mixing manifold outlets do not affect the heat performance nor, in a first approximation, do they affect the flow regime of the mixing manifold. The manifold can thus be optimized without referring to the geometry of the outlet circuits. We may point out that the various outlet temperature amplitudes in each case of Fig. 8 and Table 3 can be explained by the fact that the pack temperature varies daily with that of the test room.

Without internal devices or outlet diaphragms (case 1 in Fig. 8, Table 3), the maximum thermal fluctuation at the outlets does not exceed 1°C. Consequently, the mixing is sufficient for thermal regulation and passenger comfort. The flow regime causes a low-frequency aeroacoustic buzzing noise that is particularly harmful for passenger comfort and vibratory fatigue [15]. This noise is due to the presence of a PVB in the mixing manifold, and this has been confirmed by frequency analysis (Fig. 9). The higher amplitudes in the spectrum, around 200 and 400 Hz, correspond to the acoustical signature of the experimental setup.

The unsteady numerical simulations showed that a periodic phenomenon is present at a frequency of 34.4 Hz, instead of 39.7 Hz in the experimental data (the variation of the 3-D velocity magnitude

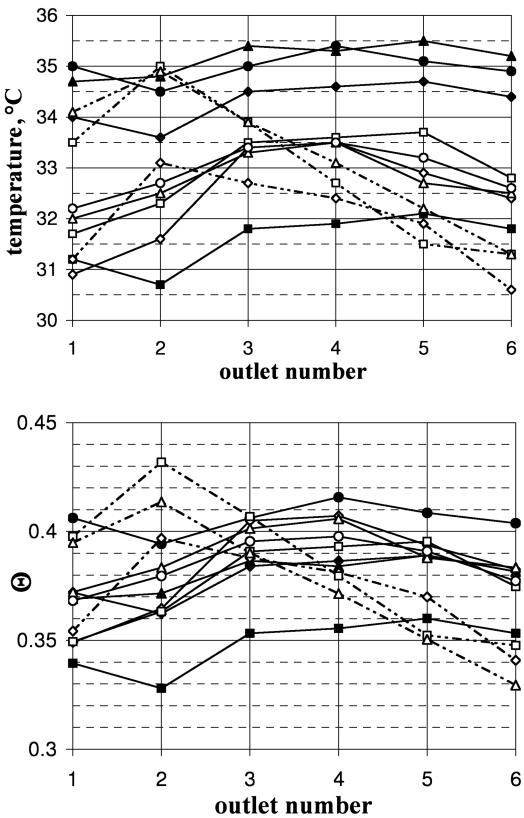

Fig. 8 Experimental manifold outlet temperature distributions.

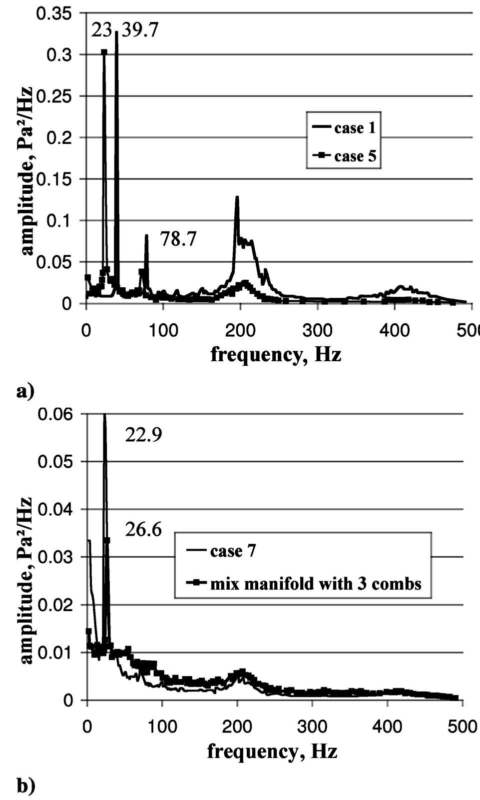

Fig. 9 Manifold outlet spectra.

for the monitoring point in the reference plane is given in Fig. 10). Contrary to other industrial configurations (swirl burners, for example), only one PVB is present [9]. The PVB corresponds to the points of maximum axial vorticity. The precessing center (Fig. 10) is not located on the mixing manifold axis [16].

A recirculation zone, precessing with the PVB, is present from the bottom to the top of the mixing manifold. In the numerical data, we noticed the occurrence of left-handed symmetry: the PVB corotates with the swirling flow, whereas the vortex core axis counter-rotates. In fact, the helical vortex core begins spiraling from the bottom of the mixing manifold, and its pitch seems to be very large (at least of the order of the mixing manifold height). Figures 11 and 12 show the axial and 3-D velocity maps, respectively, in the x = 700 mm plane (Fig. 1) whereas the vortex core coincides with each of the four points studied in Fig. 10. The PVB involves periodic increases of the axial and 3-D velocity amplitudes as the flow is squeezed between the PVB and the mixing manifold walls. This phenomenon is due to the angular momentum flux balance. The flows near the wall are encouraged by the peripheral outlets, whereas those near the axis are less so (see also Fig. 13). The global flow rate is thus confined mainly near the cylinder walls. These high axial velocities accelerate the heat transfer with the boundaries. This is why the mixing manifolds used in aircraft have external thermal insulation: to limit transfers with the outside environment. To understand the effect the near wall flow has on the mixing quality, we replaced the central zone with a cylindrical wall (175 mm diam). We noticed less pressure loss (between 6% and 28% depending on the inlet) but a higher thermal fluctuation of 8.5°C at the outlets. And so, the central zone is useful for mixing hot and cold air flows. It increases the transverse flows and ensures good mixing. The left-handed symmetry is thus beneficial to heat transfer.

Nevertheless, we noticed some discrepancies between experimental and numerical data. The thermal mixing is overestimated by the numerical simulation. We get a maximum outlet variation of 4.1°C instead of 1°C. However, cold and hot outlets seem to be predicted well.

The flow regime in aeronautical mixing manifolds corresponds to a hydrodynamic mode [17]. This has to be different from the experimental prototype self-acoustic modes to avoid any resonances which might be critical for structural coherence. The rotating structure seems not to be acoustically controlled (this phenomenon is generally present in industrial reactive burners [18]).

Further experiments showed that the PVB frequency increases with the total inlet flow rate of the mixing manifold (Fig. 14). For a square-section cylinder, Alekseenko et al. [10] found that the PVB frequency increases linearly with the total flow rate (all inlets have

Table 3 Cases tested for quantification of mixing manifold pneumatic performances

Case	Exit diaphragm, mm, scale 0.445						Internal		Reduced height	Corresponding symbols in Fig. 8
	1	2	3	4	5	6	Comb.	Diaph.		
1	——	——	——	——	——	——	——	——	——	◆ (solid line)
2	——	——	——	——	——	——	——	——	——	■ (solid line)
3	——	——	——	——	44.5	31.2	——	——	——	▲ (solid line)
4	44.5	——	31.2	——	44.5	——	——	——	——	● (solid line)
5	——	——	——	——	——	——	3	1	——	◇ (solid line)
6	——	——	——	——	44.5	31.2	3	1	——	□ (solid line)
7	——	——	——	——	——	——	3	2	——	△ (solid line)
8	——	——	——	——	44.5	31.2	3	2	——	○ (solid line)
9	——	——	——	——	——	——	——	——	17%	◇ (dashed line)
10	——	——	——	——	——	——	3	1	17%	□ (dashed line)
11	——	——	——	——	44.5	31.2	3	1	17%	△ (dashed line)

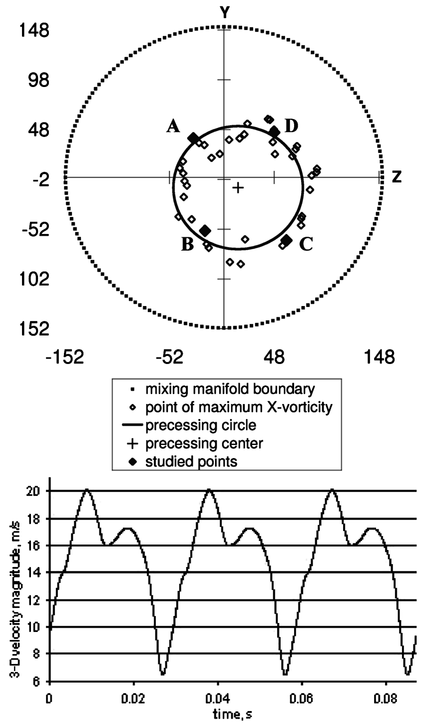

Fig. 10 3D velocity amplitude variation for a monitoring point inside the manifold (in mm).

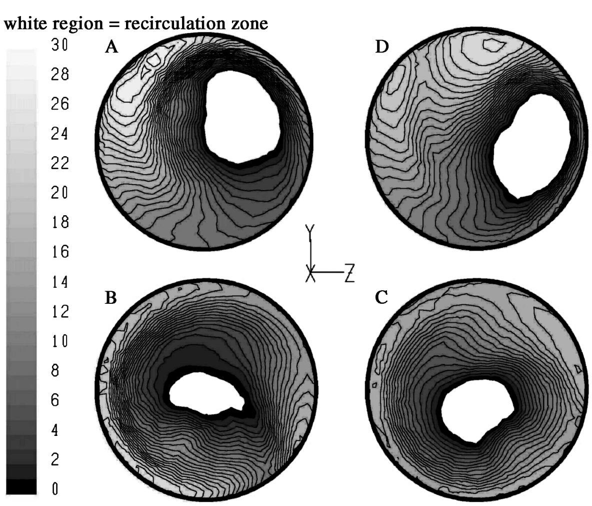

Fig. 11 Contours of axial velocity in the x = 700 mm horizontal plane.

the same flow rate). In our study, the manifold is supplied by four inlets with various flow rates, and none of them increases by the same ratio (because of the limitations of the experimental apparatus). However, the PVB frequency variation becomes quite linear for high flow rates.

The difference between cases 1 and 2 in Fig. 8, Table 3 is the different ratio set between pack and recirculation flow rates (1.6 instead of 1.4). The mixing quality is then satisfactory. Moreover, if we modify the amplitudes of the inlet flow rates (266 vs 304 l/s for the cold inlets and 202 vs 191 l/s for the hot), the mixing homogeneity then seems not to be affected (even in the presence of internal devices). Consequently, the mixing manifold is a reliable apparatus even in an emergency, such as when a fan drops out. The flow regimes (breakdown and PVB) found in mixing manifolds are stable (mainly due to the relative high Reynolds and swirl numbers, and to the presence of peripheral outlets).

Three combs and a first diaphragm were placed on the mixing manifold wall (case 5 of Table 3, Figs. 3 and 8). When internal devices were added, the mixing quality decreases, which is paradoxical because the internal devices are turbulence generators that should favor heat transfer. The maximum thermal fluctuation at the outlets is then 2.6° (and 10.1°C for the numerical results; but again, cold and hot outlets agree well). Moreover, the mixing manifold pressure loss decreases by 20% compared with reference

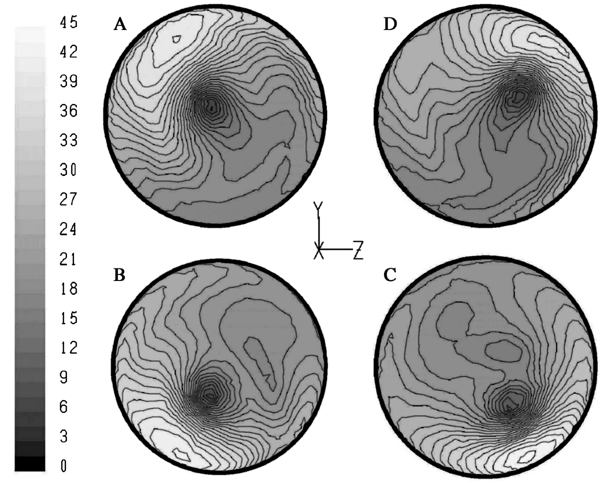

Fig. 12 Contours of 3-D velocity magnitude in the x = 700 mm horizontal plane.

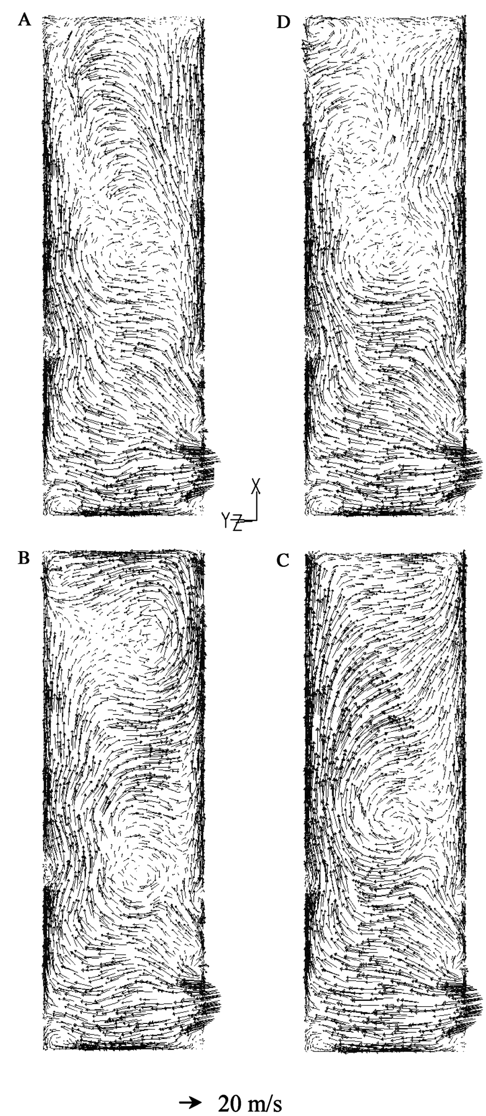

Fig. 13 2-D velocity vector diagrams in the plane 0 deg of Fig. 1.

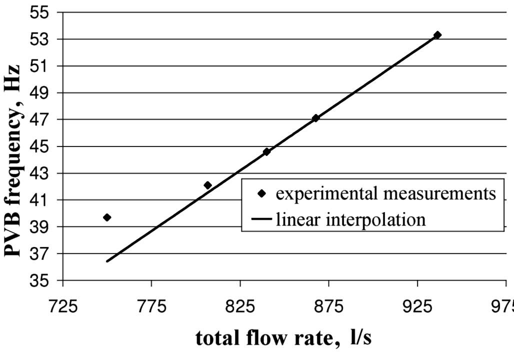

Fig. 14 Effect of total inlet flow rate on PVB frequency.

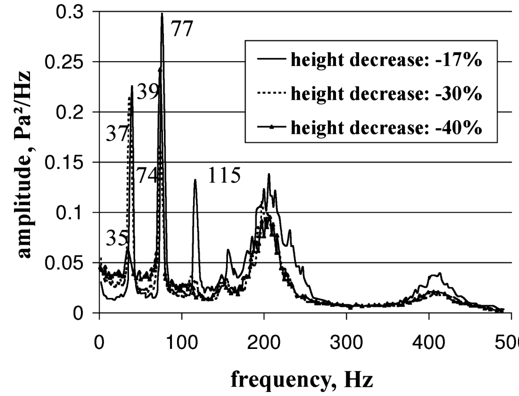

Fig. 15 Effect of mixing manifold height reduction on PVB frequency and amplitude.

case 1, for similar inlet conditions. The internal devices may thus cause a flow regime modification.

We noticed that the diaphragm creates a countercurrent along the manifold walls, improving the water flow toward the drain, thereby performing the water collection function. Again, frequency analysis (Fig. 9) shows a root (22.9 Hz) corresponding to a PVB. For a given total inlet flow, the PVB frequency decreases in the presence of internal devices and the precessing center of the PVB is moved. As in case 1, this element increases with the total inlet flow rate, but the acoustic levels remain lower, at the limit of the human ear sensitivity. The CFD simulations agree with the experimental data, and show that the transverse flows in the recirculation zone are lower in the presence of internal devices.

When a second internal diaphragm is added (case 7 of Table 3, Figs. 3 and 8), we get a good mixing process (with a maximum thermal fluctuation of 1.5°C at the outlets) without increasing the total pressure loss (rise of 2% over case 5) or the PVB frequency. This configuration is very close to one chosen for the Airbus A340-600. In fact, the low-pressure loss, the low acoustic amplitudes (Fig. 9), and the mixing quality are a satisfactory compromise with a view to meeting aeronautical specifications.

However, we might note that a manifold with only three combs offers a better maximum thermal fluctuation at the outlets, a 30% decrease in pressure loss, a low root amplitude, and a PVB frequency nearly equal to case 7 (Fig. 9). Solero and Coghe [19] describe an experimental test on a cyclone chamber. By fixing a square rod on the separator wall, they were able to avoid the PVB flow regime and decrease the pressure loss by 7%. In our study, the combs have a similar function: they reduce the pressure loss and aeroacoustic noise. For all these reasons, this configuration seems to be the best one, but it is nonetheless rejected because it does not provide the water collection function.

B. Effects of Mixing Manifold Height Reduction

When the manifold height is reduced 17%, the mixing is degraded (Fig. 8, Table 3). That is, the transverse flows in the central region of the manifold are carried over a smaller distance. A minimum manifold height seems to be required in order for these flows to be efficient. Figure 15 shows the acoustic frequency variations for a manifold with no internal devices, for different height reductions: −17, −30, and −40%. In every case, the root and the harmonic frequencies are closed. Consequently, the manifold height has no fundamental effect on the PVB frequency. However, the height reduction significantly decreases the root amplitude.

These results show that it is difficult to get good thermal mixing quality, manifold height reduction, and low acoustic noise all at once. A height reduction of 40% does not cancel the PVB but only decreases its development. We conclude that the PVB appears at the bottom of the mixing manifold around the inlet levels (probably from the shear layers). It then begins precessing and the radius of its trajectory increases with the mixing manifold height.

C. Changing the Boundary Conditions

When a central outlet (same diameter as the others) is placed at the top of the mixing manifold, it naturally exhibits a low flow rate. The mixing quality is similar to case 1, but the pressure loss decreases significantly (to about 20%). Acoustic analysis brings out the fact that no root or harmonic are present inside the manifold (only the test bench acoustic signature is discernible). We thus concluded that no aeroacoustic phenomenon were present. So, the PVB is not necessary responsible for the thermal quality. If the top outlet flow rate is too low, the PVB phenomenon reappears. The aeroacoustic noise can then be controlled by regulating the flow rate. Consequently, we have here an interesting configuration that improves passenger comfort and satisfies the aeronautical specifications.

Alekseenko et al. [10] studied the PVB phenomenon in a confined swirling flow (helical vortex with finite core). Their formula for the precession frequency can be divided into four terms. The first deals with the size of the vortex core and the curvature of its axis. The second represents the axis torsion effect. The third is the contribution due to the walls; the last reflects the effect of the velocity along the chamber axis. In the reference case, the axial velocity is limited. In the present configuration, this axial velocity seems sufficient to compensate the curvature and torsion effects. The decrease in the pressure loss again underscores the fact that the PVB phenomenon absorbs a significant amount of kinetic energy and consequently increases the manifold pressure drop.

We then put five outlets at the top of the mixing manifold in place of the central outlet. This configuration has similarities with that of the Airbus A380. The maximum thermal fluctuation at the six peripheral outlets is then satisfactory (less than 1°C), but this can reach 2.5°C for the five outlets at the top. Hot or cold air injectors are then needed to correct the temperatures. This geometry exhibits a 50% decrease in pressure loss (compared with the reference case), good mixing quality, and a qualitatively low acoustic noise (acoustic measurements show there is no root). The top outlets have poor mixing quality and heterogeneous velocities because they are supplied only from the central recirculation zone. A height reduction of 17% entails a thermal fluctuation of 3.3°C. Adding the top outlets does not offer a reduction in the spatial dimensions.

The qualification of the mixing manifold's thermal, acoustic, and pressure loss performance bettered our understanding of swirl flow regimes, boundary conditions, the effects of internal devices, and the effect of manifold height reduction. This height reduction entails a degradation of the thermal mixing for the A340-600 configuration. Complementary studies show that modifications of the peripheral outlet geometry, involving a loss of the omnidirectional symmetry, have no effect on the mixing quality or acoustic noises. Modifying the inlet geometry might thus be a better way of reducing the spatial dimensions of the mixing manifold.

V. Mixing Manifold Optimization

Aeronautical specifications are becoming more and more demanding from the weight and space allocation viewpoints. Consequently, mixing manifolds need to be reduced without degrading the thermal mixing process.

Table 4 Effect of injection angle on maximum thermal fluctuation

		Maximum thermal gap, °C			Pressure loss, Pa			Root amplitude, Pa^2/Hz
	height decrease, %	−17	−30	−40	−17	−30	−40	−17
Injection angle, deg	0	0.5	0.7	1.4	1684	1666	1676	0.51
	22.5	0.5	0.9	1.8	1654	1643	1655	0.88
	45	1.1	2.3	4.4	1712	1690	1697	0.65
	67.5	1.2	2.6	4.6	1660	1665	1656	0.07

In this study, we modified only the bottom part of the mixing manifold. Hot and cold inlets are now in the same horizontal plane, equally distributed, and alternated around the circumference. This configuration seems to benefit heat transfer. The injection angle can be varied to modify the geometric swirl number.

Table 4 shows the maximum thermal fluctuation between the various outlets, along with the pressure loss and the root amplitude for each manifold configuration, with no internal devices.

For all the manifold heights, the mixing quality deteriorates as the injection angle increases (i.e., the geometric swirl number decreases), and the pressure loss remains constant. Swirl flows are consequently more beneficial to the mixing quality than are impacting flows, corresponding to a 90 deg injection angle (Fig. 5).

Tangential inlets allow a 40% height decrease with a good mixing quality. However, the acoustic spectrum shows the presence of a PVB generating qualitative noise. For each injection angle, the PVB root and the corresponding harmonic frequencies are measured (Fig. 16). They decrease with the injection angle, which is in accordance with Syred's findings [6]. The PVB generates high acoustic noise for injection angles of less than 45 deg, and its level decreases to the audible limit beyond 45 deg. The injection angle also reduces the PVB root amplitude (Table 4). A direct tie-in can thus be established with the degradation of the thermal mixing: the PVB frequency decrease would entail lower heat and mass transfers in the mixing manifold. Nevertheless, we noticed good mixing without the presence of a PVB, in the case of the mixing manifold of the Airbus A340-600 with a central top outlet.

The preceding studies on the effects of internal devices and boundary conditions on the A340-600 geometry are not necessarily

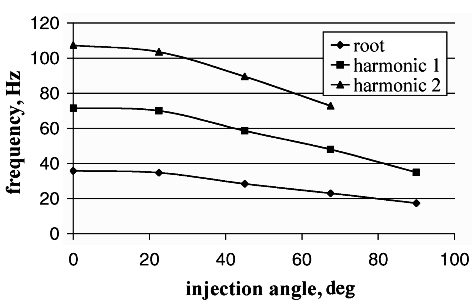

Fig. 16 Injection angle effect on PVB frequency; 17% height reduction, no internal devices.

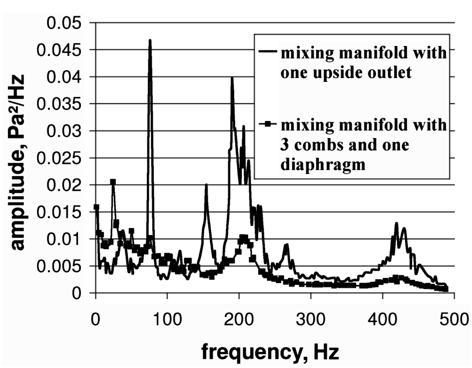

Fig. 17 Mixing manifold outlet spectra; tangential inlets in the same plane.

valid for configurations with inlets in the same plane. The following results are valid whatever the injection angle, and for a manifold height corresponding to a configuration with a maximum thermal fluctuation of 1.5°C at the outlets.

The central top outlet decreases the pressure loss by 20% but does not cause the PVB to disappear (Fig. 17). Its efficiency, from the acoustical viewpoint, is then dependent on the geometric characteristics inlets. It leads to lower axial velocities near the axis than in the A340-600 configuration (with the Ps1 inlet downward directed), and is consequently insufficient for canceling the precession frequency. Several top outlets affect the mixing quality, contrary to the A340-600 configuration, but lead to a 50% decrease in pressure loss and no acoustic noise. Three combs and one diaphragm offer good mixing without high acoustic noises (Fig. 17), or an increase in pressure loss. As a consequence, the geometrical configuration of the inlets and the manifold height have an effect on the internal devices and top outlet functions.

For all the configurations studied, the optimum configuration from the pressure loss, mixing quality, and acoustic noise viewpoints is with a 22.5 deg injection angle, a 30% height reduction, three combs, and one diaphragm. The maximum thermal fluctuation is then 1.1°C, the pressure loss is 1600 Pa, and the PVB is absent. The pressure loss is nearly equal to that of the A340-600 configuration with three combs and one diaphragm.

VI. Conclusions

This study has bettered our understanding of aeronautical air conditioning mixing manifolds. The kinetic and thermal similarity rules have been validated for a scaled-down model of the A340-600 mixing manifold configuration, which enables us to attain better experimental conditions. Several flow regimes, corresponding to heterogeneous mixing qualities, pressure losses, and acoustic noises, can be created by changing the boundary conditions. Frequency and CFD analyses underscore the presence of a PVB involving high acoustic noise but good mixing for a manifold with no internal devices. These devices damp the PVB phenomenon, thereby decreasing the pressure loss and degrading the mixing process. Left-handed symmetry and the associated precessing vortex are then penalizing for the pressure loss, but improve the mixing. The type and position of the internal devices have a nonnegligible effect on the thermal mixing, aeroacoustic noises, and water collection efficiency. With top outlets, we can cancel the PVB phenomenon and reduce the pressure loss in the manifold, but this often requires a thermal correction at the outlets. We note that the RSM can capture the PVB phenomenon. Good agreement is obtained for predicting the precession frequency. Nevertheless, experimental mapping would be needed to test the code's ability to simulate mean and instantaneous velocity maps. Moreover, large eddy simulations (LES) may be better adapted to study the PVB phenomenon.

When the height of the A340-600 mixing manifold is reduced, the mixing process is degraded but the acoustic amplitude of the PVB root is reduced (its frequency remains nearly unchanged). The geometry of the A340-600 mixing manifold was modified to meet aeronautical weight and space reduction specifications. A configuration with hot and cold inlets in the same horizontal plane, equally distributed and alternated around the circumference, with an injection angle of 22.5 deg and internal devices, leads to a 30% height reduction with good thermal mixing, low pressure loss, and no PVB. We note that the geometrical configuration of the inlets and the height of the manifold have an effect on the internal devices and top outlet functions.

Future studies will be undertaken to analyze the PVB phenomenon in detail (for breakdown characteristics and stagnation points), along with the mechanisms leading to PVB disappearance, using complementary unsteady numerical simulations (LES recommended) and PIV visualizations.

References

[1] Eggebrecht, J., Rogers, H., and Yorozu, A., Boeing, "Air Conditioning System and Air Mixing/Water Separation Apparatus Therein," U.S. Patent 4517813, filed 21 May 1985.

[2] Klepper, O. H., "Heat Transfer Performance of Short Twisted Tapes," *Heat Transfer American Institute of Chemical Engineers Symposium*, Vol. 69, No. 131, 1973, pp. 87–93.

[3] Yowakim, F. M., and Kind, R. J., "Mean Flow and Turbulence Measurements of Annular Swirling Flows," *Journal of Fluids Engineering*, Vol. 110, No. 33, 1988, pp. 257–263.

[4] Yilmaz, M., Comakli, O., Yapici, S., and Sara, O. N., "Heat Transfer and Friction Characteristics in Decaying Swirl Flow Generated by Different Radial Guide Vane Swirl Generators," *Energy Conversion and Management*, Vol. 44, No. 18, 2003, pp. 283–300.

[5] Gupta, A. K., Lilley, D. G., and Syred, N., *Swirl Flows*, Abacus, Tunbridge Wells, U.K., 1984.

[6] Syred, N., "Review of Oscillation Mechanisms and the Role of the Precessing Vortex Core (PVC) in Swirl Combustion Systems," *Progress in Energy and Combustion Science*, Vol. 32, No. 2, 2006, pp. 93–161.

[7] Razgaitis, R., and Holman, J. P., "Survey of Heat Transfer in Confined Swirl Flows," *Future Energy Production Systems: Heat and Mass Transfer Processes*, Vol. 2, Jan. 1976, pp. 831–866.

[8] Martemianov, S., and Okulov, V. L., "Heat Transfer Enhancement in Swirl Pipe Flows," *International Journal of Heat and Mass Transfer*, Vol. 47, Nos. 10–11, 2004, pp. 2379–2393.

[9] Lucca-Negro, O., and O'Doherty, T., "Vortex Breakdown: a Review," *Progress in Energy and Combustion Science*, Vol. 27, No. 4, 2001, pp. 431–481.

[10] Alekseenko, S. V., Kuibin, P. A., Okulov, V. L., and Shtork, S. I., "Helical Vortices in Swirl Flow," *Journal of Fluid Mechanics*, Vol. 382, 1999, pp. 195–243.

[11] "Measurement of Fluid Flow in Closed Conduits. Velocity Area Method for Regular Flows Using Pitot Static Tubes," Association Française de Normalisation, Norm ISO 3966 (NFX 10-112),Sept. 1977.

[12] "*Fluent 5: User's Guide*," Vol. 2, Fluent, Lebanon, NH, 1998, Chap. 9.

[13] Leclaire, B., Jacquin, L., and Sipp, D., "Effet d'une Tuyère Convergente sur un Écoulement Tournant," *17th Congrès Français de Mécanique*, Vol. 244, Sept. 2005.

[14] Lehugeur, B., and Gilliéron, P., "Caractérisation des Tourbillons Longitudinaux de Sillage de Véhicules Automobiles," *17th Congrès Français de Mécanique*, Vol 152, Sept. 2005.

[15] Kutateladze, S. S., Volchkov, E. P., and Terekhov, V., *Aerodynamics, Heat and Mass Transfer in Confined Vortex Flows*, Inst. of Thermophysics, Novosibirsk, Russia, 1987.

[16] Fick, W., Griffiths, A. J., and O'Doherty, T., "Visualisation of the Precessing Vortex Core in an Unconfined Swirling Flow," *Optical Diagnostics in Engineering*, Vol. 2, No. 1, 1997, pp. 19–31.

[17] Lartigue, G., Roux, S., Benoit, L., Poinsot, T., Meier, U., and Berat, C., "Studies of Unsteady Cold and Reacting Flow in a Swirled Combustor Using Experiments, Acoustic Analysis and Large Eddy Simulations," *Propulsion and Engines Combustion Colloquium*, 2003.

[18] Selle, L., Benoit, L., Poinsot, T., Nicoud, F., and Krebs, W., "Joint Use of Compressible Large-Eddy Simulation and Helmholtz Solvers for the Analysis of Rotating Modes in an Industrial Swirled Burner," *Combustion and Flame*, Vol. 145, Nos. 1–2, Jan. 2006, pp. 194–205.

[19] Solero, G., and Coghe, A., "Experimental Fluid Dynamic Characterization of a Cyclone Chamber," *Experimental Thermal and Fluid Science*, Vol. 27, No. 1, 2002, pp. 87–96.